Superlattices and Microstructures 75 (2014) 222–232

Contents lists available at ScienceDirect

Superlattices and Microstructures

journal homepage: www.elsevier.com/locate/superlattices

Excitons in a surface quantum well

M. Arulmozhi *, A. Anitha

Department of Physics, Jayaraj Annapackiam College for Women (Autonomous), Periyakulam 625 601, Theni District, Tamilnadu, India

ARTICLE INFO

Article history:
Received 2 December 2013
Received in revised form 20 July 2014
Accepted 21 July 2014
Available online 1 August 2014

Keywords:
III–V Semiconductors
Quantum wells
Excitons and related phenomena

ABSTRACT

Binding energies of excitons in a Surface Quantum Well (SQW) composed of vacuum/GaAs/$Al_xGa_{1-x}As$ as a function of wellwidth are calculated. The effect of non-parabolicity is considered by using an energy dependent effective mass. The effect of mass anisotropy and the effect of image charges which arise due to the large dielectric discontinuity at the vacuum/GaAs interface are also considered. The average distances of the electron $\langle z_e \rangle$ and the hole $\langle z_h \rangle$ from the vacuum/GaAs interface, with and without image charges and the integrated probability of finding an electron and a hole inside the well are also calculated. The results agree well with the available experimental data.

© 2014 Elsevier Ltd. All rights reserved.

1. Introduction

Studies on thin crystalline films, surfaces and ultrathin multilayer heterostructures are of considerable interest for the past many years because of their technological importance [1] and also due to the possibility of many new effects [2–4] shown by these systems. Quantum wells (QW) with varied potential profiles have become possible with experimental techniques [5]. Many interesting features are noted in the behavior of excitons in such QW when compared to that in a bulk semiconductor [6].

Cen et al. [7] obtained appreciable correction to the binding of excitons in a symmetrical rectangular quantum well (RQW) formed by GaAs–AlAs and GaAs–ZnSe with and without an applied magnetic field along the growth axis. Mosko et al. [8] reported exciton binding energy in a vacuum barrier QW, <vacuum/GaAs/vacuum>. They showed that interface polarization is expected to repel the charge carriers causing a deadlayer near the interface. Photoluminescence at room temperature and

* Corresponding author.
E-mail addresses: arulpkm@yahoo.co.in (M. Arulmozhi), anitha.jayarani@gmail.com (A. Anitha).

http://dx.doi.org/10.1016/j.spmi.2014.07.027
0749-6036/© 2014 Elsevier Ltd. All rights reserved.

cathodoluminescence studies of Muth et al. [9] showed a strong emission peak corresponding to the lowest bound state of the GaN surface quantum well and a correlation was made to the shift in surface quantum-well emission energy and the thickness of the GaN capping layer, which was varied from ~15 to 40 Å. Wang and Yang [10] studied the quantum dynamics of electrons in a surface quantum well in the time domain with autocorrelation of wave packet.

Quang et al. [11] presented the theory of an ad hoc mechanism for electron scattering in heavily-doped zinc oxide surface quantum wells and showed that the carriers must be extra scattered in the in-plane from roughness-induced fluctuations in the donor density. Niculescu and Eseanu [12] studied the exciton effects on the interband absorption spectra in near-surface square and semiparabolic quantum wells under intense laser field taking into account the correct dressing effect for the confinement potential and electrostatic self-energy due to the repulsive interaction between carriers and their image charges. Silkin et al. [13] studied low-energy plasmons in ultrathin films of silver in the thickness regimes where the surface states as well as quantum-well states must play significant roles. Gippius et al. [14] investigated the exciton transition and binding energies in near-surface InGaAs/GaAs quantum wells (NSQW) theoretically and experimentally by photoluminescence and photoluminescence excitation spectroscopy.

Diarra et al. [15] calculated the electronic states of donor and acceptor impurities in nanowires and showed that the ionization energy of the impurities is strongly enhanced with respect to the bulk, above all when the wires are embedded in a material with a low dielectric constant. Corfdir and Lefebvre [16] studied the influence of the surface and of the dielectric mismatch on the binding energy of donor atoms in GaN, ZnO and GaAs nanostructures and showed that due to the combination of these two effects, the binding energy does not monotonically decrease from the center to the surface. Tran Thoai et al. [17] calculated the binding energies of excitons in a finite barrier QW including the effects of image charges. Pierre et al. [18] measured a strong enhancement in the ionization energy of the dopant by the close proximity of materials with a different dielectric constant than the host semiconductor. Bjork et al. [19] demonstrated the deactivation of doping atoms in silicon nanostructures caused by a dielectric mismatch between the wire and its surroundings.

Experimental work of Parks et al. [20] in a SQW with structure vacuum/GaAs/$Al_xGa_{1-x}As$ showed the presence of states localized above the single quantum barrier in the $Al_xGa_{1-x}As$ layer. Their results showed a difference between the theoretical values and the experimentally measured transition energies obtained from the electromodulation spectra and this difference was attributed to the exciton binding energy. In this paper, an attempt is made to calculate the exciton binding energies in such a SQW using a variational approach. The effect of non-parabolicity on the transition energies, mass anisotropy and the role of image charges which arise due to the large difference in the dielectric constants on either side of the interface between vacuum and GaAs, in such a SQW are considered. A comparison is made with the experimental data and available results for potential wells of different shapes.

2. Theory

One-band effective mass and envelope function approximation is employed in the description of electrons and holes in semiconductor heterostructures.

2.1. Well states

The potential profiles for the electron and the hole in a SQW is taken to be of the form

$$V_i(z_i) = \begin{cases} \infty & z_i < 0 \\ 0 & 0 < z_i < L \\ V_{oi} & z_i > L \end{cases} \tag{1}$$

where V_{oi} is the barrier height (i stands for e or h for electron or hole, as the case may be). The values of the potential well heights V_{oe} and V_{oh} are determined as $0.65\Delta E_g$ and $0.35\Delta E_g$ [21] respectively, where the bandgap difference ΔE_g is related to the Al composition x [22] by

$$\Delta E_g = 1.155x + 0.37x^2 eV$$

L is the wellwidth and $z_i = z_e$ or z_h for the electron and the hole respectively. The wavefunctions for the electron and the hole states are of the form

$$\psi_i(z_i) = \begin{cases} 0 & z_i < 0 \\ A\sin\alpha_i z_i & 0 < z_i < L \\ Be^{-\beta_i z_i} & z_i > L \end{cases} \tag{2}$$

where A is a normalization constant and B is related to A through the continuity of ψ at $z_i = L$ as $B = Ae^{\beta_i L}\sin\alpha_i L$. The α's and β's are given by

$$\alpha_i = \sqrt{\frac{2m^* E_i}{\hbar^2}} \quad \text{and} \quad \beta_i = \sqrt{\frac{2m^*(V_{oi} - E_i)}{\hbar^2}} \tag{3}$$

where E_i is the well state energy ($i = e$ or h for electron or hole respectively), $m^* = m_e^*$ for the electron and $m_\pm^*$ for the holes. m_e^* is the effective mass of the conduction electron and $m_\pm^*$ is the heavy (+) or light (−) hole mass for motion along the z-direction.

The transcendental equation to be solved for the quantum well states is obtained by matching the wavefunction given in Eq. (2) and its first derivative at $z_i = L$, which is true when the effective mass mismatch between GaAs and $Ga_{1-x}Al_xAs$ is neglected. One gets after simplification and substitution for α_i and β_i,

$$\pm\left(\frac{E_i}{V_{oi}}\right)^{1/2} = \sin(\sqrt{E_i}L) \tag{4}$$

The transcendental equation for the electron states is obtained by including the non-parabolicity for the conduction band [23,24] by an expression for the energy dependent effective mass as

$$\pm\left(\frac{E_e}{V_{oe}}\right)^{1/2} = \sin\left[\left(\sqrt{\frac{m_e^*(E_e)E_e}{m_e^*}}\right)L\right] \tag{5}$$

The $m_e^*(E_e)$ is taken to be $m_e^*(E_e) = 0.0665\left(1 + \frac{0.0436E_e + 0.236E_e^2 - 0.147E_e^3}{0.0665}\right)$ where E_e is in eV.

2.2. Ground state of excitons

The Hamiltonian for an exciton in a SQW is given by

$$H = -\left[\frac{1}{\rho}\frac{\partial}{\partial\rho}\rho\frac{\partial}{\partial\rho} + \frac{1}{\rho^2}\frac{\partial^2}{\partial\phi^2}\right] - \frac{\mu_\pm^*}{m_e^*}\frac{\partial^2}{\partial z_e^2} - \frac{\mu_\pm^*}{m_\pm^*}\frac{\partial^2}{\partial z_h^2} + V_e(z_e) + V_h(z_h) - \frac{2}{r} \tag{6}$$

where $r = \sqrt{\rho^2 + |z_e - z_h|^2}$. The unit of energy is the effective Rydberg $R_\pm^* = \frac{\mu_\pm^* e^4}{2\hbar^2\varepsilon_1^2}$ and the unit of length is the effective Bohr radius $a_\pm^* = \frac{\hbar^2\varepsilon_1}{\mu_\pm^* e^2}$, where ε_1 is the dielectric constant of GaAs.

$\mu_\pm^*$ is the reduced effective mass of the *hh* exciton and the *lh* exciton. It is calculated, in the isotropic case, as $\frac{1}{\mu_\pm^*} = \frac{1}{m_e^*} + \frac{1}{m_\pm^*}$ and in the anisotropic case, using Kohn-Luttinger parameters [25], $\gamma_1 = 7.36$ and $\gamma_2 = 2.57$, as $\frac{1}{\mu_\pm^*} = \frac{1}{m_e^*} + \frac{1}{m_o}(\gamma_1 \pm \gamma_2)$ and $\frac{1}{m_\pm^*} = \frac{1}{m_o}(\gamma_1 \mp 2\gamma_2)$ where m_o is the free electron mass.

The potential profile is as given in Eq. (1). The trial wavefunction for the Wannier exciton (associated with the lowest electron and hole states) in the SQW is taken to be of the form

$$\psi = \begin{cases} 0 & z_e, z_h < 0 \\ A_2\sin\alpha_e z_e \sin\alpha_h z_h e^{-ar} & 0 < z_e, z_h < L \\ B_2 e^{-\beta_e z_e} e^{-\beta_h z_h} e^{-ar} & z_e, z_h > L \end{cases} \tag{7}$$

where 'a' is a variational parameter and the α's and β's are as in Eq. (3). The continuity conditions at $z_e = L$ and $z_h = L$ give

$$B_2 = A_2 e^{\beta_e L} e^{\beta_h L} \sin \alpha_e L \sin \alpha_h L \tag{8}$$

leaving A_2 to be fixed by the normalization condition.

2.3. Effect of image charges

At the GaAs/Al_xGa_{1-x}As interface, we have neglected the effects due to the effective mass mismatch [14,26–28] and the dielectric constant mismatch [26–28] which are expected to be small, when we consider the binding energies. But image charges arises due to the large mismatch of the dielectric constant at the interface between vacuum and GaAs. Now the electron sees not only the hole but also its own image charge and that of the hole; similar is the case or the hole. Hence the Coulomb interaction between an electron and a hole is no longer isotropic. The image charge of an electron or a hole is expressed as [29]

$$q_i' = \frac{\varepsilon_1 - \varepsilon_2}{\varepsilon_1 + \varepsilon_2} q_i \tag{9}$$

where the dielectric constant in the GaAs well is ε_1 and that in vacuum is ε_2. $i = e$ for electron and h for hole. $q_e = -e$ and $q_h = e$.

Unlike the symmetrical wells, the dielectric constant mismatch is considered only at the single vacuum/GaAs interface in the SQW (the small mismatch at the GaAs/Al_xGa_{1-x}As interface is neglected). This leads to the formation of only one image each for the electron and the hole. The image potential hence has the simple form when compared to the image potentials used in other cases. For example in Ref. [8], a symmetrical vacuum barrier quantum well (vacuum/GaAs/vacuum) has been considered and for this case, there will be an infinite number of images and the image potential involves an infinite sum. In a similar fashion, Ref. [7] deals with the dielectric constant mismatch at the two interfaces in a rectangular quantum well. The image potential reduces to the expression used in our work when we consider a single interface. The additional potential in the Hamiltonian, when the image charge is considered, is given by

$$V_a = \frac{q_e q_h'}{\varepsilon_1 \sqrt{\rho^2 + (z_e + z_h)^2}} + \frac{q_e' q_h}{\varepsilon_1 \sqrt{\rho^2 + (z_e + z_h)^2}} + \frac{q_e q_e'}{\varepsilon_1 2 z_e} + \frac{q_h q_h'}{\varepsilon_1 2 z_h} \tag{10}$$

Taking the unit of energy as the effective Rydberg and the unit of length as the effective Bohr radius, the image potential now becomes

$$V_a = K \left[\frac{-4}{\sqrt{\rho^2 + (z_e + z_h)^2}} + \frac{1}{z_e} + \frac{1}{z_h} \right] \tag{11}$$

where $K = \frac{\varepsilon_1 - \varepsilon_2}{\varepsilon_1 + \varepsilon_2}$. The new Hamiltonian for the exciton is now given by

$$H_{image} = H + V_a \tag{12}$$

The exciton binding energy is determined by evaluating $\langle H_{image} \rangle$ and minimizing it w.r.t the variational parameter 'a' using the trial wavefunction given in Eq. (7). It is verified that the dielectric enhancement of electron and hole energy levels is very less for SQW (i.e., only the exciton energy levels are affected by the image charges and not the electron and hole energy levels). So only the value of the variational parameter 'a' will be different with and without the image charges. The binding energy of the exciton is now given by

$$B.E = E_e + E_h - \langle H_{image} \rangle_{\min} \tag{13}$$

The average distances of the electron $\langle z_e \rangle$ and the hole $\langle z_h \rangle$ from the vacuum/GaAs interface, with and without image charges, are also calculated, using the value of the variational parameter 'a' corresponding to $\langle H_{image} \rangle_{\min}$ and $\langle H \rangle_{\min}$ respectively as

$$\langle z_e\rangle = \frac{\int\int\int\int \psi^* z_e \psi dz_e dz_h \rho d\rho d\phi}{\int\int\int\int \psi^* \psi dz_e dz_h \rho d\rho d\phi}$$
$$\langle z_h\rangle = \frac{\int\int\int\int \psi^* z_h \psi dz_e dz_h \rho d\rho d\phi}{\int\int\int\int \psi^* \psi dz_e dz_h \rho d\rho d\phi} \quad (14)$$

where ψ is as given in Eq. (7). The integrated probability of finding an electron and a hole inside the well is calculated as

$$P = \int_0^{2\pi}\int_0^L\int_0^\infty \psi^*\psi\rho d\rho dz d\phi \quad (19)$$

The effect due to the effective mass mismatch is neglected, an effect which is expected to be small.

3. Results and discussion

Effective masses of electron (m_e^*), heavy hole (m_+^*) and electron (m_-^*); reduced masses of heavy hole exciton (μ_+^*) and light hole exciton (μ_-^*) calculated in the isotropic and anisotropic cases mentioned in Section 2.2; dielectric constants of GaAs (ε_1) and vacuum (ε_2) used in the calculations are given in Table 1.

The experimental samples used in Ref. [20] have the Al composition $x = 0.3$ and the wellwidth $L = 150$ Å, 400 Å and 1650 Å. The quantum well states for the electron and the hole are determined for various wellwidths by solving the transcendental Eq. (4). Taking E_g(GaAs) = 1.5192 eV, the transition energies between the hole levels in the valence band and the electron levels on the conduction band are calculated. It is found that there is a good agreement between our results and the experimental results reported by Parks et al. [20] for electron-*hh* transition energies. These values corresponding to the experimental samples are given in Table 2.

In Fig. 1, the variation of the binding energy of the ground state of a *hh* exciton and a *lh* exciton as a function of the wellwidth L, is displayed. The binding energy initially increases with the decrease of wellwidth until it reaches a maximum and then decreases quite rapidly. This behavior is similar for both the *hh* exciton and the *lh* exciton. The reason for this is that as L is reduced, the exciton wavefunction is compressed in the QW, leading to increased binding. However, beyond a certain value of L, the spread of the exciton wavefunction into the surrounding $Al_xGa_{1-x}As$ layer becomes more important. This makes the binding energy decrease as L is reduced further. Therefore, a turnover is observed in the binding energy of the exciton as the wellwidth is decreased. This behavior is similar to the case of finite QW of all shapes.

The correction for exciton binding energy applied by Parks et al. [20] for an agreement between their theoretical and experimental values of transition energies in SQW, as estimated by Nelson et al. [32], is very large compared to our results. But the wellwidth range is not the same in Parks et al. [20] and Nelson et al. [32]. The maximum value of the binding energy is also comparable with that in QWs of other shapes. Table 3 gives the comparative values in different QWs.

From Table 3, it is seen that the turnover in the binding energy in the case of SQW happens at a value of L greater than that in the case of RQW [31] and smaller than that in a $|z|^{2/3}$ [28] QW. This

Table 1
Material parameters used in the calculations.

Parameters	Isotropic [30]	Anisotropic [25]
m_e^*	$0.0665m_o$	$0.067m_o$
m_+^*	$0.34m_o$	$0.45m_o$
m_-^*	$0.094m_o$	$0.08m_o$
μ_+^*	$0.05562m_o$	$0.04m_o$
μ_-^*	$0.03895m_o$	$0.05m_o$
ε_1	13.2	13.2
ε_2	1	1

Where m_o is the free electron mass.

Table 2
Ground state energies and transition energies for experimental sample wellwidths [20].

L (Å)	Ground state energies (meV)			Transition energies (eV)	
	Electron	*hh*	*lh*	Electron-*hh*	Electron-*lh*
150	20.52	3.12	16.39	1.5428	1.5561
400	3.26	0.50	2.68	1.5223	1.5251
1650	0.20	0.03	0.17	1.5194	1.5196

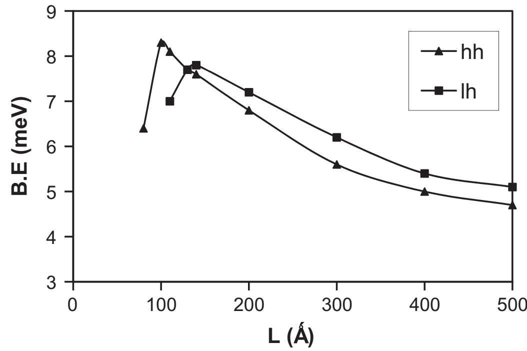

Fig. 1. Variation of the binding energy of the ground state of a heavy hole exciton (*hh*) and a light hole exciton (*lh*) without the image charges as a function of wellwidth (L) with anisotropic masses.

Table 3
Binding energies of excitons in QWs of different shapes.

Well type	$(E_{hh})_{max}$ (meV)	$(E_{lh})_{max}$ (meV)	Turnover value at L (Å)		Crossover at L (Å)
			L_{hh}	L_{lh}	
RQW [31]	9.4	9.2	25	50	50
$\|z\|^{2/3}$ [28]	7.4	5.3	225	260	250
SQW	8.3	7.8	100	140	130

shows that the exciton wavefunction penetrates into the barrier of a SQW much more than in the case of RQW and much less than the $|z|^{2/3}$ QW, as L is reduced.

It is also seen that the binding energy of the *lh* exciton $E_B(lh)$ is larger than that of the *hh* exciton $E_B(hh)$ for L greater than a certain critical value L_c at which they become equal. This shows that the *lh* exciton is more bound than the *hh* exciton until the crossover wellwidth is reached. For values below L_c, $E_B(lh)$ is smaller than $E_B(hh)$. This crossover is essentially due to the mass anisotropy involved. i.e., $m^*_+ > m^*_-$ while $\mu^*_+ < \mu^*_-$. Also $E_B(lh)$ increases less rapidly than $E_B(hh)$ since more of the *lh* exciton wavefunction tends to spillover into the surrounding $Al_xGa_{1-x}As$ layer, than the *hh* exciton wavefunction.

Fig. 2 shows the variation of the binding energy of the ground state of a *hh* exciton and a *lh* exciton as a function of the wellwidth L using an exciton Hamiltonian with isotropic masses where $m^*_+ > m^*_-$ and $\mu^*_+ > \mu^*_-$ (for anisotropic case $\mu^*_+ < \mu^*_-$). Here the *hh* exciton is more bound than the *lh* exciton for all wellwidths and hence there is no crossover as expected.

The variation of the integrated probability of finding the *hh* and *lh* exciton inside the SQW as a function of the wellwidth L is shown in Fig. 3. It is found that the probability shows a rapid decrease at nearly the wellwidth at which the binding energy shows a turnover. This is because the turnover is mainly due to the spilling over of the exciton wavefunction into the surrounding $Al_xGa_{1-x}As$ layer. No crossover is found in the *hh* and *lh* exciton probabilities because the crossover seen in the binding

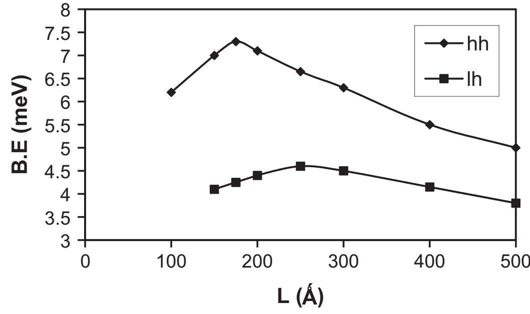

Fig. 2. Variation of the binding energy of the ground state of a heavy hole exciton (*hh*) and a light hole exciton (*lh*) without the image charges as a function of wellwidth (*L*) with isotropic masses.

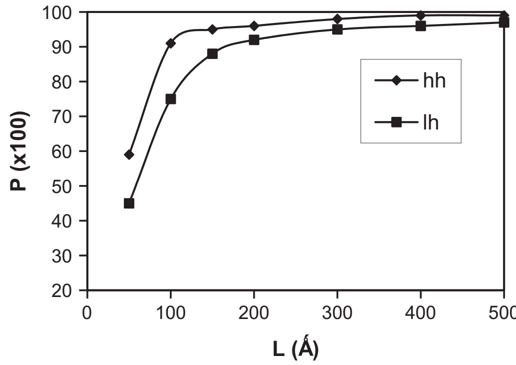

Fig. 3. Variation of the integrated probability of finding a heavy hole exciton (*hh*) and a light hole exciton (*lh*) inside a SQW as a function of wellwidth *L* without the image charges.

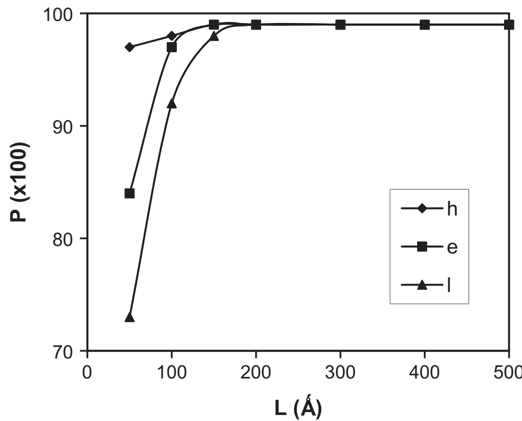

Fig. 4. Variation of the probability of finding an electron (*e*), a heavy hole (*h*) and a light hole (*l*) inside a SQW as a function of wellwidth *L* without the image charges.

energies shown in Fig. 1, is mainly due to the mass anisotropy and the fact that $m_+^* > m_-^*$ while $\mu_+^* < \mu_-^*$.

In Fig. 4, the variation of the probability of finding an electron, a *hh* and a *lh* inside the SQW as a function of the wellwidth *L*, is shown. The *hh* is found to have the highest probability, then comes the electron and finally the *lh* for a particular value of *L*. The barrier height for the electron (conduction band) is V_{oe} = 246.87 meV and for the holes (valence band), it is V_{oh} = 132.93 meV. Considering the valence band, since the effective mass of the *hh* is larger than that of the *lh*, the probability of finding the *hh* inside the well is greater than that of the *lh*, for a particular value of *L*. Though the effective mass of the electron is smaller than that of the *lh*, its probability inside the well is greater because of the larger barrier height.

The variation of the binding energies of the *hh* and *lh* excitons including the image charges as a function of the wellwidth is shown in Fig. 5. It is seen that the binding energies are significantly reduced, when image charges are included. In contrary, Gippius et al. [14] have reported that image charge effects in NSQW lead to an increase in exciton binding energy. The difference in the behavior may be due to the following variations in the calculations. (i) Non-inclusion of the layer next to InGaAs QW by Gippius et al. [14] (ii) choice of the potential levels for the QW and (iii) use of anisotropic masses of the excitons by the present authors.

We also find that the turnover in the binding energy of the excitons, as the wellwidth is reduced, is at a larger value of the wellwidth, when the effect of image charges is included. The reason again is due to the fact that the penetration of the exciton wavefunction into the surrounding $Al_xGa_{1-x}As$ layer becomes more. The repulsion of electron and hole by the polarization at the vacuum/GaAs interface assists the above penetration. The binding energies of the excitons with and without the image charges, the turnover and crossover wellwidths are presented in Table 4.

The difference in the binding energy (ΔE) of the excitons with and without the image charges is calculated and its variation with the wellwidth *L* is shown in Fig. 6. When these results are compared with those reported by various authors [7,8,15–19], the following differences are noted. The reasons for these differences are also given.

1. In the references mentioned, symmetric semiconductor nanostructures are considered where the electron and hole suffer repulsion due to the image charges arising due to the polarization at both the interfaces, which increases the confinement and hence the binding energy. But for the asymmetric SQW studied by the present authors, repulsion is experienced only at the single vacuum/well interface having dielectric discontinuity, which decreases the confinement and hence the binding energy.
2. There is no turnover in the difference in binding energy with and without the image charge as the wellwidth decreases, for a symmetrical rectangular QW [7] as well as for the vacuum barrier QW [8] up to $L \sim 50$ Å. But for a SQW, a turnover is observed in the difference in binding energy of the excitons with and without the image charges as the wellwidth decreases. This difference can again be attributed to the asymmetrical nature of the polarized interfaces.

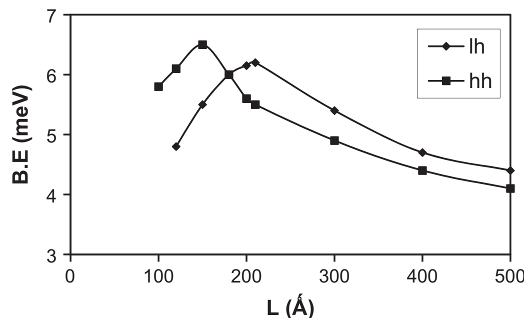

Fig. 5. Variation of the binding energy of the ground state of a heavy hole exciton (*hh*) and a light hole exciton (*lh*) with the image charges as a function of wellwidth (*L*) with anisotropic masses.

Table 4
Maximum binding energies of excitons with and without the image charges, turnover and crossover wellwidths for SQW.

Image charges	$(E_{hh})_{max}$ (meV)	$(E_{lh})_{max}$ (meV)	Turnover value at L (Å)		Crossover at L (Å)
			L_{hh}	L_{lh}	
Absent	8.3	7.8	100	140	130
Present	6.5	6.2	150	210	180

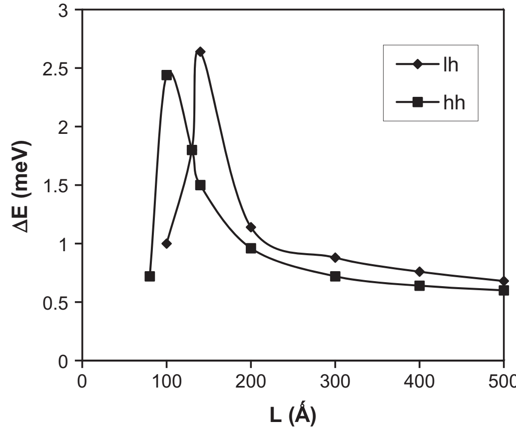

Fig. 6. Variation of the binding energy of the ground state of a heavy hole exciton (*hh*) and a light hole exciton (*lh*) with the image charges as a function of wellwidth (L) with isotropic masses.

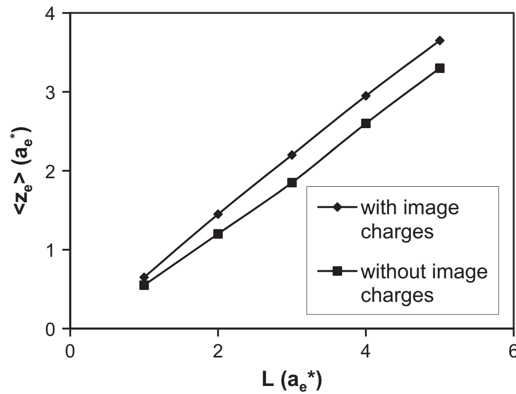

Fig. 7. Variation of the average distance of the electron $\langle z_e \rangle$ from the vacuum/GaAs interface with and without the image charges as a function of wellwidth L. Effective Bohr radius of electron, a_e^* = 98.7 Å.

Fig. 7 shows the variation of the average distance of an electron $\langle z_e \rangle$ calculated with the *hh* exciton wavefunction, from the vacuum/GaAs interface, with and without the image charges as a function of the wellwidth, L. It is found that as the wellwidth increases, the electron moves away from the vacuum/GaAs interface. When the effect of image charges is included, the electron is initially attracted, when the wellwidth is less than that corresponding to maximum binding energy. Thereafter, the electron is repelled and the force of repulsion increases as the wellwidth increases.

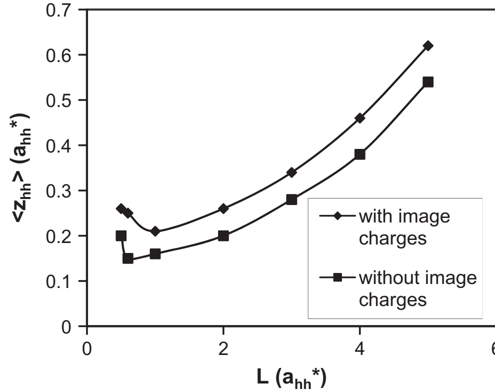

Fig. 8. Variation of the average distance of the heavy hole $\langle z_{hh}\rangle$ from the vacuum/GaAs interface with and without the image charges as a function of wellwidth *L*. Effective Bohr radius of heavy hole, a_{hh}^{*} = 14.7 Å.

The variation of the average distance of the heavy hole $\langle z_{hh}\rangle$ from the vacuum/GaAs interface with and without the image charges, as a function of the wellwidth L is shown in Fig. 8. Unlike the electron, the heavy hole is repelled for all wellwidths, when the effect of image charges is included. It is also found that the force of repulsion initially decreases when the wellwidth is less than that corresponding to maximum binding energy. It is noted that the *hh* is always close to the vacuum/GaAs interface, when compared to the average electron distance.

In Fig. 9, the variation of the average distance of the light hole $\langle z_{lh}\rangle$ from the vacuum/GaAs interface with and without the image charges as a function of the wellwidth L, is displayed. The variation is similar to that of the electron.

On comparison, it is seen that, for a particular value of L, the effect of image charges is the highest in the case of a *lh*, then comes the electron and then the h. This is consistent with the integrated probability shown in Fig. 4. When the probability of finding a charge carrier inside the well is larger, it is less affected by the image charges. The interface polarization is expected to repel the charge carriers causing deadlayer near the interface, which will be free of excitons.

The notion of deadlayer, discussed in the literature [6], in the context of semi-infinite solids, can be considered for the SQW. The latter differs from single interface in having a confining potential also. Hence the repulsion due to the polarization charge on the interface giving rise to an electric field does not push the charge carriers to large distance, as in the semi-infinite solids. The deadlayer in a SQW is thus expected to be small. Our calculations of $\langle z_e\rangle$ and $\langle z_{hh}\rangle$ give a qualitative idea of the dead layer in a SQW. For example, for the wellwidth of 5 a_{+}^{*}, $\langle z_e\rangle$ and $\langle z_{hh}\rangle$ are increased respectively by about 0.3 a_{+}^{*}

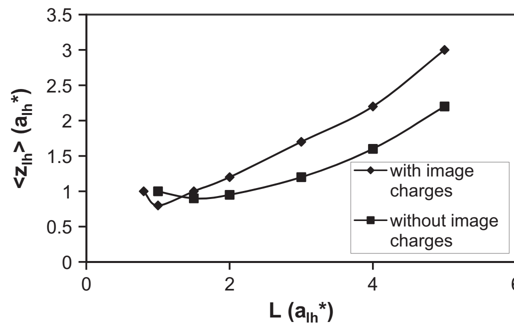

Fig. 9. Variation of the average distance of the light hole $\langle z_{lh}\rangle$ from the vacuum/GaAs interface with and without the image charges as a function of wellwidth *L*. Effective Bohr radius of light hole, a_{lh}^{*} = 82.7 Å.

and 0.1 a_+^*, when the image charges are included. These are about 10% of $\langle z_e \rangle$ and $\langle z_{hh} \rangle$, without the image charges.

4. Conclusion

Exciton binding energies in a SQW composed of vacuum/GaAs/$Al_xGa_{1-x}As$ as a function of wellwidth are calculated including the effect of non-parabolicity and image charges. The effect of image charges in a SQW is different from that in a symmetrical rectangular QW where the carriers experience repulsion by the image charges arising due to the polarization at both the interfaces and is compelled to be at the center of the QW. But in the SQW, they are repelled by the image charge at the single vacuum/GaAs interface only. Calculation of the average distances of the electron $\langle z_e \rangle$ and the hole $\langle z_h \rangle$ from the vacuum/GaAs interface, with and without image charges and the integrated probability of finding an electron and a hole inside the well show that the deadlayer in a SQW is smaller compared to semi-infinite solids.

Acknowledgements

The authors thank the University Grants Commission, New Delhi, India for the financial support through Major Research Project (No. F. 42-836/2013 (SR) dated 22.03.2013) and the authorities of Jayaraj Annapackiam College for Women (Autonomous), Periyakulam, Theni District, Tamil Nadu, India for the encouragements.

References

[1] Handbook of Surfaces and Interfaces of Materials, H.S. Nalwa (Ed.), vol. 4, Solid Thin Films and Layers, Copyright©2001 by Academic Press.
[2] R. Dingle, Festkorper-Probleme (Advances in Solid State Physics), vol. XV, 21, Pergamon Vieweg, Braunschweig, 1975.
[3] T. Ando, A.B. Fowler, F. Stern, Rev. Mod. Phys. 54 (1982) 437.
[4] R.R. Prange, S.M. Gorvin (Eds.), The Quantum Hall Effect, Springer Verlag, New York, 1987.
[5] Claude Weisbuch, Borge Vinter, Quantum Semiconductor Structures (Fundamentals and Applications), Academic Press Inc. (Harcourt Brace Jovanovich Publishers), Boston, 1991.
[6] R. Del Sole, A. D'Andrea, A. Lapiccirella (Eds.), Excitons in Confined Systems, in: Proceedings of the International Meeting, Rome, Italy, 1987. (Springer Verlag, Berlin, 1987).
[7] J. Cen, R. Chen, K.K. Bajaj, Phys. Rev. B 50 (1994) 10947.
[8] M. Mosko, D. Munzar, P. Vagner, Phys. Rev. B 55 (1997) 15416 (A misprint has to be corrected: x^k should read $x^{|k|}$ in Eqs. (3) and (4)).
[9] J.F. Muth, X. Zhang, A. Cai, D. Fothergill, J.C. Roberts, P. Rajagopal, J.W. Cook, Appl. Phys. Lett. 87 (19) (2005) 192117 (3 pages).
[10] Li.-Fei. Wang, Guang.-Can. Yang, Chin. Phys. B 18 (6) (2009) 2523–2528.
[11] Doan Nhat Quang, Le Tuan, Nguyen Thanh Tien, J. Appl. Phys. 107 (12) (2010) (123709-123709-8).
[12] E.C. Niculescu, N. Eseanu, Eur. Phys. J. B 79 (3) (2011) 313–319.
[13] V.M. Silkin, T. Nagao, V. Despoja, J.P. Echeverry, S.V. Eremeev, E.V. Chulkov, P.V. Echenique, Phys. Rev. B 84 (16) (2011) 165416.
[14] N.A. Gippius, A.L. Yablonskii, A.B. Dzyubenko, S.G. Tikhodeev, L.V. Kulik, V.D. Kulakovskii, A. Forchel, J. Appl. Phys. 83 (10) (1998) 5410–5417.
[15] M. Diarra, Y.-M. Niquet, C. Delerue, G. Allan, Phys. Rev. B 75 (2007) 045301.
[16] P. Corfdir, P. Lefebvre, J. Appl. Phys. 112 (2012) 106104.
[17] D.B. Tran Thoai, R. Zimmermann, M. Grundmann, D. Bimberg, Phys. Rev. B 42 (9) (1990) 5906–5909.
[18] M. Pierre, R. Wacquez, X. Jehl, M. Sanquer, M. Vinet, O. Cueto, Nat. Nanotechnol. 5 (2010) 133.
[19] M.T. Bjork, H. Schmid, J. Knoch, H. Riel, W. Riess, Nat. Nanotechnol. 4 (2009) 103.
[20] C. Parks, A.K. Ramdas, M.R. Melloch, G. Steblovsky, L.R. Ram Mohan, H. Luo, Solid State Commun. 92 (1994) 563.
[21] G. Duggan, H.I. Ralph, K.J. Moore, Phys. Rev. B 32 (1985) 8395.
[22] H.J. Lee, L.Y. Juravel, J.C. Wooley, A.J. Springthorpe, Phys. Rev. B 21 (1980) 659.
[23] K. Jayakumar, S. Balasubramanian, M. Tomak, Phys. Rev. B 33 (1986) 4002.
[24] S. Chaudhuri, K.K. Bajaj, Phys. Rev. B 29 (1984) 1803.
[25] J.M. Luttinger, W. Kohn, Phys. Rev. 97 (1955) 869.
[26] S. Chaudhuri, K.K. Bajaj, Solid State Commun. 52 (12) (1984) 967–970.
[27] A.M. Elabsy, Phys. Rev. B 46 (4) (1992) 2621–2624.
[28] M. Arulmozhi, S. Balasubramanian, Phys. Rev. B 51 (4) (1995) 2592–2595.
[29] J.D. Jackson, Classical Electrodynamics, second ed., John Wiley & Sons, Singapore, 1974. p. 147–148.
[30] D.F. Nelson, R.C. Miller, C.W. Tu, S.K. Sputz, Phys. Rev. B 21 (1980) 659.
[31] R.L. Greene, K.K. Bajaj, D.E. Phelps, Phys. Rev. B 29 (1984) 1807.
[32] D.F. Nelson, R.C. Miller, C.W. Tu, S.K. Sputz, Phys. Rev. B 36 (1987) 8063.